METHODS OF SPACE RADIATION DOSE ANALYSIS WITH APPLICATIONS TO MANNED SPACE SYSTEMS

R. W. Langley and M. P. Billings

McDonnell Douglas Astronautics Company
Huntington Beach, California

ABSTRACT

The full potential of state-of-the-art space radiation dose analysis for manned missions has not been exploited. Point doses have been overemphasized, and the critical dose to the bone marrow has been only crudely approximated, despite the existence of detailed man models and computer codes for dose integration in complex geometries. The method presented makes it practical to account for the geometrical detail of the astronaut (which typically provides as much protection to the internal organs as does the vehicle) as well as the vehicle. This paper discusses the major assumptions involved and presents the concept of applying the results of detailed proton dose analysis to the real-time interpretation of on-board dosimetric measurements.

INTRODUCTION

Present state-of-the-art methods for space radiation dose analysis have been routinely used on a number of existing and proposed manned space systems. The experience gained in applying the involved analytical techniques, the extent of agreement between analytical results and experimental investigations, and the increased knowledge of the space radiation environment have resulted in reasonable confidence in the ability to predict space radiation doses to specific points in a vehicle used for manned missions. A summary of the state-of-the-art and current practices is given in reference 1; the current experimental approach and experimental results are summarized in reference 2.

The most troublesome and important space-radiation protection problem continues to be that of biological hazard, and one of the most difficult aspects of the biological hazard problem is onboard dose monitoring. The most stringent biological dose criterion is generally that associated with the internally distributed blood-forming organs (BFO) or bone marrow, and the critical radiation environment for practically all manned missions is protons, both solar protons and trapped protons. It is in the context of these generalizations that this paper is presented.

SCOPE OF PRESENT DISCUSSION

Considerable theoretical and experimental effort has gone into establishing and improving the accuracy of present methods for calculating point doses, and there seems little to be gained in further efforts along these lines at this point. Emphasis should instead be placed on improving the application of these methods to preflight and in-flight dose estimation. The two major points of this paper concern (1) astronaut self-shielding of internally distributed organs, and (2) the realistic interpretation of on-board dosimetry.

The aspect of dose analysis that in particular deserves more attention is the effective utilization of detailed astronaut (as well as vehicle) geometry. Available methods for estimating point doses are rather accurate for geometrically well-defined systems, particularly for protons. However, the application of these methods to the estimation of doses to the internally distributed organs (such as the BFO) of a mobile astronaut has not exploited the available potential for obtaining accurate dose estimates. This is because the complexity involved in the combined geometrical mockup of a vehicle and a mobile detailed man-model requires excessive time and effort to integrate over the several space and time variables involved in the dose integrations. The geometrical complexity involved can be appreciated by viewing a model or mockup of the NASA Space Station and considering a man-model described by over 2200 geometrical shapes (ref. 3). The alternative to precise "brute-force" integration that has seen widespread application is the use of gross simplifications, such as characterizing the average BFO dose by a few point doses calculated at a 5-cm depth in a phantom. Because the protection provided to the BFO by the vehicle may well be less than that provided by the self-shielding of the astronaut and because the protection provided by both is highly spectrum dependent, this degree of simplification largely negates the care normally taken with other aspects of dose analysis; for example, in specifying the quality factor and the vehicle mass distribution. The approach presented utilizes the available capability of detailed man-models and circumvents the problems of excessive effort on the one hand and excessive crudeness on the other.

Another area requiring attention is the application of the significant dose analysis capability that has been developed over the past ten years to the problem of on-board dose monitoring. The uncertainty associated with preflight dose estimation, in decreasing order of importance, is due to (1) the space environment encountered during the mission, (2) the distribution of mass providing protection, and (3) methods of radiation transport and dose analysis (ref. 4). In situ measurements, however, remove the major source of uncertainty (that associated with the radiation environment) so that the main dose uncertainties are then due to the combined mass distribution of the vehicle and astronaut. An accurate treatment of the overall geometrical arrangements of mass will therefore enhance the overall accuracy of dose estimation. It is precisely this sensitivity of dose to mass distribution

for manned space systems that makes direct dosimetric measurements impractical in real-time dose monitoring. An approach is presented for making practical use of available dose analysis tools and detailed man-models to provide a means of realistic, real-time interpretation of on-board dosimetric measurements.

REPRESENTATION OF ASTRONAUT GEOMETRY AND MOTION

The usual method of estimating dose to the BFO (for example) of a mobile astronaut has been to create a geometrical mockup of a man-model inside the space system, and to perform dose integrations about several points in the body, each of which is erroneously assumed to be at a uniform depth of 5 g/cm^2, for several man-model locations within the vehicle. This procedure represents a compromise in the spatial and astronaut time-line integrations, and makes it impractical to use both a detailed mockup of the vehicle and a detailed man-model of the type described in reference 3.

The alternative method that has been developed yields improved dose estimates by accounting for the actual organ distribution within the body, the dose distribution within the organ, and the astronaut time-line. Such a detailed integration is made practical by decoupling the mass distribution of the vehicle from the mass distribution of the astronaut. This is accomplished by using mass-distribution data generated from an existing detailed man-model to express the shielding effect of the body on critical organ dose. Typical mass distributions for the BFO are shown as curves 2 and 3 in figure 1. When fully implemented, each curve generated would be volume-averaged over some portion of the BFO; that is, each curve would represent a part of the BFO (e. g., upper limbs, lower limbs, ribs and trunk, spinal column, and skull) rather than a point, as in figure 1. Other distributed radiation-sensitive organs (e. g., the gut) could be treated similarly, and if it turns out to be important, these data should be generated for both the standing and the sitting positions. Doses to the skin and lens of the eye are essentially surface doses for which body self-shielding can be adequately estimated without the explicit use of a man-model (ref. 5).

The mass distribution data of figure 1 were generated by tracing several hundred randomly selected rays. Curve 1 is the time-averaged distribution for a simplified astronaut time-line made up of five dwell stations in the Skylab vehicle that account for most of the time, with the remainder of the time spent in uniform transit between the station locations. A more detailed time-line could be constructed from measured data like those presented in reference 6. Curve 1 was generated with the use of the SIGMA code (ref. 7). Curves 2 and 3 were generated for an isolated, standing astronaut with the MEVDP code (ref. 8), which contains the man-model of reference 3.

Such astronaut mass distribution data have been combined with the vehicle mass-distribution data in two ways. One way of combining them in a dose analysis has been to use them in the same manner that a man-model is now used; i. e., using the organ mass distribution to calculate depth doses for each ray as it is traced, and then summing the desired results. Another way, which is more efficient when integration over astronaut time-line is involved, has been to generate the time-line averaged vehicle mass distribution separately (such as indicated by curve 1, figure 1), and then obtain the final results by convoluting the mass distributions and integrating over the dose kernels and organ response (i. e., the distribution factor or other dose-modifying factors). This latter approach is illustrated in figure 2, in which the utilization of man-model geometrical mockup is shown in dashed lines to indicate that it is used only once and not in every dose analysis.

The advantages of the decoupling method over the present method are:

1. Dose estimates to such organs as the BFO are significantly more accurate and realistic.

2. Application of the available detailed man-model capability is made practical.

3. Much greater detail in dose analysis for either the final design or preliminary analysis is obtainable with a small increase in engineering effort and with reduced computer time.

4. Ability to interpret data from on-board monitoring is enhanced.

The implementation of the proposed method involves the following assumptions: (1) the effects of an astronaut's actual orientation on dose are not significant on the average, (2) the error involved in using a single reference material in the dose kernels is not significant, and (3) the vehicle mass distribution at a point is representative of a region of space (occupied by one or more organ segments, as necessary). A series of calculations indicates the validity of the first two assumptions. The third assumption is not considered restrictive, since vehicle mass distributions can be generated on the basis of a single coordinate time-line for an astronaut or as many as one coordinate time-line for each organ mass-distribution curve of interest, depending on how a specific situation affects the accuracy.

EVALUATION OF DOSE INTEGRATION TECHNIQUES

A 44-region geometrical mockup of a manned space station (ref. 9) and a simple man-model consisting of one elliptical cylinder for the head and another for the trunk were used to perform a series of calculations with the SIGMA code. Doses were calculated for a point representing the lens of the eye at a single man-model location. A surface dose was chosen to emphasize any effects of man-model orientation with respect to the vehicle. Two proton spectra were used: an exponential rigidity spectrum (P_o = 91 MV) for solar cosmic rays and an exponential energy spectrum (E_o = 94 MEV) for trapped protons. The calculations illustrate several possible approaches to dose analysis, indicate the effects of vehicle/man-model orientation, and provide a comparison between random and systematic ray-tracing. The results are summarized in table 1.

The conventional method of dose analysis corresponds to case 1, for which a combined geometrical mockup is used for both the vehicle and the astronaut, thereby maintaining a fixed specific vehicle/man-model orientation. The method of dose integration uses a systematic sectoring and ray-tracing procedure. Case 2 provides a comparison with case 1 with respect to random versus systematic ray-tracing. This is of interest because the more variables or dimensions involved in an integration, the more advantageous the Monte Carlo technique will be from a computational standpoint. Therefore, the generation of astronaut mass distributions and the dose integration for a detailed time-line using random ray-tracing (i.e., Monte Carlo integration) would significantly reduce the computation cost relative to that required for systematic ray-tracing (i.e., direct numerical integration) for the same precision. Table 1 shows that, even for a simple example with integrations employing 500 rays, Monte Carlo integration is superior; a more complex integration would show a greater advantage. Case 2 was also run, using 5,000 rays to obtain an accurate result as a basis for comparison. In this case, the solar cosmic-ray dose calculated by the Monte Carlo technique (using 500 rays) was more accurate than that obtained with systematic ray-tracing.

For dose integrations of reasonable accuracy, at least 100 rays are required (as shown later). For this many rays, there is no mathematical or practical justification for elaborately sectoring and tracing rays through sector centroids; this approach is attractive only because it corresponds to a mental construct. For systematic ray-tracing, parts of the solid angle space will always be inaccessible to rays; this is not true of random sampling. If there are thin regions or "windows," the bias used in sectoring can easily be applied to Monte Carlo integration, although this is unnecessary for all sizable space vehicles examined to date (including several configurations of MORL, MOL, Skylab, and the Space Station).

Cases 3 and 4 are similar to cases 1 and 2, except they demonstrate the use of a man-model mass distribution (defined by a histogram) applied as indicated in figure 2. The doses are slightly higher for cases 3 and 4 because of the lack of a fixed vehicle/man-model orientation. The higher doses thus obtained are to be expected because the minimum in the astronaut mass distribution is exposed to the direction of maximum flux (as well as all other directions). It is also true that the larger conservative dose is the desirable one to use except in a special (and unlikely) situation in which an astronaut's orientation is severely and reliably restricted for a significant period of time.

Case 5 indicates how little computation is involved in dose integration aside from ray-tracing computations. Once mass distributions are available, it is a trivial matter for a large computer to perform the dose integrations, and the amount of time involved is independent of geometrical complexity. The vehicle histogram used in case 5 was generated from the ray-tracing analyses performed for case 4. Therefore, the dose results from case 5 should, and do, agree with the case 4 results, in which some portions of the mass distribution data were obtained by ray-tracing instead of sampling a histogram.

Summarizing, the conclusions supported by table 1 are as follows:

1. The doses for oriented cases closely agree with those for unoriented cases, the unoriented cases giving slightly higher doses because the use of a separate man-model mass distribution exposes the minimum mass thickness to the direction of maximum flux; use of a surface dose in the examples emphasizes this effect. Because of the unlikelihood of being able to confidently predict a nonuniform astronaut orientation in most phases of the astronaut time-line, and because an unoriented man model will usually yield a slightly conservative dose, this assumption is generally desirable.

2. The use of random ray-tracing for performing dose integration or generating mass distributions is virtually always advantageous, relative to direct numerical integration, even for a one- or two-variable integration, such as the ones performed here, where the two variables are spherical angular coordinates. When the vehicle mass distribution is calculated for a detailed astronaut time-line, the use of random sampling in time and solid angle to establish the origin and direction of rays is much more efficient than the conventional systematic-sectoring procedure.

CONVERGENCE OF DOSE INTEGRATION

A general aspect of dose calculations that relates to the above discussion is the convergence of the dose estimate with the number of rays traced and the associated uncertainty in the dose estimate. The standard deviations in table 1 indicate consistent convergence, and assuming that the number of rays traced is large enough for the central-limit theorem to apply, confidence limits and corresponding dose intervals can be readily determined by using a normal distribution with the calculated variance.

The rate of dose convergence decreases as the steepness of the dose attenuation kernel increases, so that a soft solar cosmic-ray spectrum converges slower than a relatively hard trapped-proton spectrum. The McDonnell Douglas DACP code was used to investigate the statistics of a dose estimate using the idealized but realistic mass distribution of figure 3 and the 12 November 1960 solar-flare event (ref. 10). DACP performs repetitive convolutions of probability density functions by numerical integration to obtain exact statistical results, as described in reference 11.

The dose probability distributions obtained for three sample sizes (i.e., number of rays traced) are shown in figure 4. These curves represent the frequency of results that can be obtained with all possible combinations of rays, for this particular case. For 128 rays, a very good approximation to a normal distribution is obtained (i.e., the central-limit theorem applies).

Figure 5 shows the convergence in terms of confidence levels as a function of the number of rays in a sample. For example, for a 90-percent confidence level, the actual dose has a 90-percent probability of falling somewhere between the 5-percent confidence limit curve and the 95-percent confidence limit curve. These curves can be calculated by assuming a normal distribution for sample sizes greater than approximately 100 rays.

It is concluded that Monte Carlo dose integration converges as the calculated variance implies for reasonable sample sizes (greater than approximately a hundred rays). For typical mass distributions, this is true for both random and systematic ray tracing. For this example, figure 5 shows that 1,500 rays are required to obtain a dose that is 99-percent probable of being within ±1 percent of the actual (theoretical) dose. It is emphasized that for Monte Carlo integration, the statistics are essentially the same for a single point dose or for a dose calculated for a detailed astronaut time-line. This is because for typical vehicles the average mass distribution does not vary so drastically from point to point that the rate of convergence is significantly affected by including the effect of a time-line. This is in marked contrast to conventional dose analysis, which requires convergence for each of a number of point doses, which are then appropriately summed.

VALIDITY OF EQUIVALENT ALUMINUM CONCEPT

In implementing the foregoing dose evaluation technique, it is extremely advantageous to represent proton dose attenuation kernels in terms of a reference material like aluminum. While the use of equivalent aluminum seems generally to be accepted for preliminary analysis, the question often arises about its validity for detailed analysis, particularly with regard to secondary nucleon dose.

Briefly, the equivalent aluminum concept refers to the practice of performing charged-particle dose-transmission calculations through a single reference material, usually taken to be aluminum, and using these results to describe the dose transmission through any laminated arrangement of different materials. Its application simply involves modifying the actual mass density of a shield material by its relative stopping power, which is the (practically energy-independent) ratio of the stopping power of the material to that of aluminum. This relationship must be used to give accurate results for primary proton dose; expressing the material in actual areal density is not adequate.

The question of validity must be answered in terms of the environment, materials, and calculational methods relevant to the subject. Four cases, which were chosen for analysis, represent fairly extreme but reasonable arrangements of dissimilar materials that might be encountered in a manned space system. These cases were analyzed with the CHARGE code (ref. 12), which compares well with ORNL NTC code results (ref. 13). For these cases, a typical solar proton spectrum (exponential rigidity spectrum with P_o = 91 MV) was used, and the results were compared to those for an aluminum shield. This energy spectrum is soft enough for secondary nucleon dose to be dominant at shield thicknesses approaching 50 g/cm^2, thus posing a rather severe test.

The results are shown in figure 6, which also describes the shield configurations. The aluminum represents vehicle structure, the water represents tissue, the polyethylene represents stored food and waste, and the iron represents equipment. The curves, which show only a 26-percent difference at 50 g/cm^2 are surprisingly similar considering that the dose at 50 g/cm^2 is approximately 90 percent due to secondary neutrons. Similar curves for solar cosmic-ray primary proton dose and for total dose from a typical trapped proton spectrum (not shown) are represented within a few percent by a single curve, equivalent aluminum shield thicknesses up to greater than 50 g/cm^2. Little difference for the primary proton dose would be expected because the functional dependence of stopping power with particle energy is nearly the same for all materials. A large difference in total dose, however, and particularly for dose equivalent, might be expected when secondary neutron dose dominates, as it does for typical solar cosmic-ray spectra and large shield thicknesses, because neutron production and attenuation are material dependent. Fortunately, as indicated by figure 6, this is not the case.

One reason for this fortunate coincidence is that the density correction factor for proton stopping power is also approximately correct for neutron attenuation. Figure 7 shows the relative stopping power of some materials. Also shown is the approximate relationship for the macroscopic neutron removal cross section, which varies inversely as the cube root of the atomic number (except for hydrogen). Because these relationships are similar, the same material density correction factor is applicable to both phenomena for the range of material thicknesses of interest.

Another reason is that secondary neutron production in common materials is not strongly material dependent. It varies a factor of two between aluminum and lead, and differs by only 25 percent between aluminum and iron, as indicated in figure 8. For the cases shown in figure 6, about two-thirds of all neutron secondaries were formed in the first 2 g/cm^2 of aluminum The small differences among the cases at 50 g/cm^2 are due primarily to the differences in neutron production among the materials beyond 2 g/cm^2.

The conclusion drawn from these calculations is that the use of equivalent aluminum based on relative stopping power in proton dose calculations is sufficiently accurate for the detailed design of manned spacecraft. This is because the relatively small error in the dose kernel at large shield thicknesses is unimportant to the total dose because most of the dose involves transmission through only a few g/cm^2. In addition, the spread in the curves in figure 6 is only 26 percent at 50 g/cm^2, well within the uncertainty of any calculational technique when secondary nucleon dose is dominant.

It should be noted that the negligible error indicated by this comparison is in terms of total dose, the quantity of interest. The comparison given in reference 14 is presented as a function of proton energy, which resolves (calculated) variations that are insignificant in their contribution to total dose.

ROLE OF DETAILED DOSE ANALYSIS IN REAL-TIME DOSE MONITORING

Detailed dose analyses have a proper role in real-time interpretation of on-board dose-monitoring information, as well as in the more commonly applied area of preflight dose prediction. Direct on-board measurement of the dosimentric quantities of interest (i.e., critical organ dose) is not feasible, and dose analyses must be performed to accurately relate the data that can be measured to the dosimetric quantities on which mission decisions are based. The techniques discussed previously, particularly the technique for making effective use of detailed man-model geometric data, can be applied to generate the required relationship between, for example, spectrometer measurements and expected organ response.

Solar cosmic rays provide the primary impetus for establishing a dose-monitoring system that can assess the dose and dose rate that have been received and that can project the dose and dose rate to be expected (ref. 15). There is a distinct possibility of exceeding emergency doses when one considers solar cosmic-ray environments for orbital missions with inclinations greater than 40 degrees (ref. 16), or for interplanetary missions. Because operational decisions based on dose-monitoring information can result in severe restrictions or even in mission abort, it is necessary to be as definite as possible about interpreting dosimetric data in terms of actual organ dose and anticipated organ response. For practical reasons, the significant geometrical factors cannot be accounted for by direct measurement, but can be determined only by using the results of detailed calculations to properly interpret the measurements that can be made. Regardless of how carefully dose, LET, or any other similar quantity is measured at a point or at several points, either on a phantom fixed in the vehicle or on the astronaut, these data alone give only a vague indication of actual BFO dose from solar cosmic rays. The dose behind 5 g/cm^2, regardless of whether it is measured by a tissue-equivalent dosimeter with good scattering geometry or whether it incorporates other refinements, does not adequately represent actual BFO dose from solar cosmic rays (although it is not unreasonable for neutrons and gamma rays). Because of the complexity of the geometrical factors involved, a precise correlation of such measurements with actual dose or human response can be established only by detailed dose analysis. (A discussion of some of the problems and requirements of dosimetry for manned vehicles is given in reference 17; a more general survey is given in reference 18.)

For dose calculations to be made, the radiation environment at some point in the vehicle must be known. That is, the flux intensity and energy spectrum must be known; it has not been established that incident flux anisotropy is important, and an attempt to account for it in any detail would complicate things considerably. Incident flux, differential in energy, can be measured directly by a proton spectrometer or it can be inferred from depth-dose measurements in a phantom. In either case, the flux at a location can easily be described as a piece-wise representation so that doses anywhere in the vehicle or astronaunt can then be easily correlated in real time by using the parametric results of detailed calculations. Instrument design, optimum dosimetry location, and interpretation of redundant information are important considerations in the design of a dose-monitoring system, but they are not the subject of this discussion. The point of this discussion is to introduce the idea that combining the versatility of proton-dose analysis with the reality of direct measurements can alleviate some of the difficulties of dosimetry.

GENERAL TECHNIQUE FOR INTERPRETATION OF DOSE MONITORING DATA

The on-board measurements of proton spectra will provide data on the flux in several energy bands or channels at a location in the vehicle, as indicated by the histogram in figure 9. These in situ radiation-environment data can then be converted to astronaut organ dose or dose equivalent through use of a dose transfer function (DTF) that is generated by using detailed dose analysis techniques, but is expressed only in terms of the measured data, i.e., flux magnitude and energy spectrum. To minimize the error in the dose estimation, the DTF must represent these data as a continuous function. The discontinuous data can be converted to a continuous function (as indicated in figure 9) by assuming a functional representation within each channel. The form is relatively unimportant and can be a power law in energy, an exponential in rigidity, or some other form for the proton environment. It can be shown that the measured data can be quickly converted to a continuous spectrum.

For an isotropic incident flux, which is piece-wise fitted, with a spectral parameter for each channel, a total dose response can easily be obtained by applying the DTF. The DTF consists, for this example, of I+2 curves (if extrapolations outside the two spectrometer energy limits are used) where I is the number of spectrometer channels. The curves are the normalized dose per channel as a function of the spectral parameter, as shown in figure 10. If there are J dose responses (e.g., BFO dose, eye dose, etc.), the DTF for this example would be J(I+2) curves similar to the curves shown in figure 10. For the jth dose response, the dose would be given by

$$D_j = \sum_{i=0}^{I+1} \psi_i \, D_{ij} \, (\alpha_i)$$

where ψ_i is the flux in channel i, where D_{ij} is the DTF curve for channel i and dose response j, and where α_i is the spectral parameter of channel i. This same idea can as easily be applied to depth-dose measurements, rather than spectrometer measurements, since a given depth-dose curve represents a unique proton spectrum.

With this approach, the DTF can include any level of detail in its generation, without complicating its expression or use. The use of a continuous piece-wise spectrum defined by a spectral parameter simplifies the dose conversion and reduces the error that can be introduced by using a flux-to-dose conversion, which is a continuous function of energy.

The accuracy of the doses thus predicted could be improved by normalizing them to a small, battery-operated, active, personal dosimeter. That is, the BFO dose would be scaled to get the value

$$D_B = D_B^C \left(\frac{D_S^M}{D_S^C} \right)$$

where D_B is the BFO dose estimate, D_B^C is the BFO dose calculated from measured data, D_S^M is the the surface dose measured by the personal dosimeter, and D_S^C is the surface dose calculated from measured data. The value D_B could, of course, represent either accumulated dose or instantaneous dose rate, and D_B^C could be used for both an average time-line and for specific fixed locations. Since all the detailed dose analyses required to construct the DTF would be precalculated, the simple operations involved in the application of the DTF could be performed by a small on-board computer. If necessary, it is probably practical to perform the conversion by hand, using nomograms.

CONCLUSIONS AND RECOMMENDATIONS

The following conclusions have been made:

1. Accurate dose estimates require accounting for:
   a. Organ distribution within the body.
   b. Dose distribution within an organ.
   c. Astronaut time-line.
2. A practical method of implementing detailed dose analyses is to decouple vehicle and astronaut mass distributions.
3. Monte Carlo ray-tracing is generally superior to systematic sectoring.
4. The equivalent aluminum concept is adequate for proton dose kernels.
5. A DTF using spectral parameters can provide rapid, real-time, in situ dose conversion.

The following are recommended:

1. Mass distribution should be generated for radiation-sensitive organs.
2. The role of dose analysis as it relates to dose monitoring should be extended to include the described DTF technique on future manned space missions.

CREDIT

Work described in this paper was conducted by the McDonnell Douglas Astronautics Company under the Independent Research and Development Account No. S. O. 80205-009.

REFERENCES

1. Langley, R. W.: Space Radiation Protection. NASA SP 8054, June 1970.
2. Janni, J. F.; and Holly, F. E.; Editors: The Current Experimental Approach to the Radiological Problems of Spaceflight. Aerospace Medicine, Vol. 40, No. 12, December 1969, pp. 1439-1567.
3. Kase, P. G.: Influence of Detailed Model of Man on Proton Depth Dose Calculations. Proceedings of this symposium.
4. Fortney, R. E.: Flight Experiment Shielding Study (FESS) Satellite Data Analysis. Report AFWL-TR-68-108, Air Force Weapons Laboratory, April 1969.
5. Hill, C. W.; Simpson, K. M., Jr.; and Ritchie, W. B.: Physical and Biological Dose Calculations for Proton and Alpha Fluxes Incident on a Shielded Man Model. Proceedings of the Special Sessions on Radiation Transport and Biological Effects, ANS-SD-4, pp. 69-78, 1966.
6. Goodman, M.; and Middleton, W. C.: Crew Locomotion Disturbances in a Space Cabin Simulator. Journal of Spacecraft and Rockets, Vol. 6, No. 10, October 1969, pp. 1207-1209.
7. Jordan, T. M.: SIGMA, a Computer Program for Space Radiation Dose Analysis Within Complex Configurations. Report DAC-60878, McDonnell Douglas Astronautics Company, November 1967.
8. Liley, B.; and Hamilton, S. C.: Modified Elemental Volume Dose Program (MEVDP). AFWL-TR-69-68, August 1969.
9. Billings, M. P.: Optimal Shield Mass Distribution for Space Radiation Protection. Proceedings of this symposium.
10. Baker, M. B.: Geomagnetically Trapped Radiation. AIAA J., Vol. 3, No. 9, September 1965, pp. 1567-1579.
11. Yucker, W. R.: Solar Cosmic Ray Hazard to Interplanetary and Earth-Orbital Space Travel. Proceedings of this symposium.
12. Yucker, W. R.; and Lilley, J. R.: CHARGE Code for Space Radiation Shielding Analysis. Report DAC-62231, McDonnell Douglas Astronautics Company, April 1969.
13. Scott, W. W.; and Alsmiller, R. G., Jr.: Comparisons of Results Obtained with Several Proton Penetration Codes - Part II, ORNL RSIC-22, June 1958.

14. Case, R.: Techniques Used for the Calculation of Space Radiation Dose. Aerospace Medicine, Vol. 40, No. 12, December 1969, pp. 1455-1461.

15. Baker, M. B.; Santina, R. E.; and Masley, A. J.: Modeling of Solar Cosmic Ray Events Based on Recent Observations. AIAA J., Vol. 7, No. 11, November 1969. pp. 2105-2110.

Table 1

RESULTS FROM VARIOUS DOSE INTEGRATION METHODS

CASE	VEHICLE DESCRIPTION (1)	MAN MODEL DESCRIPTION (2)	METHOD OF INTEGRATION	CDC-6500 COMPUTER TIME (SEC)	DOSE (RAD) SOLAR COSMIC RAYS	DOSE (RAD) TRAPPED PROTONS	VEHICLE/MAN MODEL ORIENTATION
1	GEOMETRIC	GEOMETRIC	SYSTEMATIC	27.2	54.0 (8%)(4)	24.4 (5%)	ORIENTED
2	GEOMETRIC	GEOMETRIC	RANDOM	26.7 250.1	58.8 (6%) 59.7 (2%)(5)	24.6 (3%) 25.1 (1%)(5)	ORIENTED
3	GEOMETRIC	HISTOGRAM (3)	SYSTEMATIC	27.8	58.3 (7%)	27.6 (4%)	UNORIENTED
4	GEOMETRIC	HISTOGRAM	RANDOM	28.1	64.3 (6%)	27.1 (3%)	UNORIENTED
5	HISTOGRAM	HISTOGRAM	RANDOM	4.1	63.9 (6%)	28.3 (3%)	UNORIENTED

NOTES

(1) GEOMETRICAL MOCKUP OF 44-REGION VEHICLE.

(2) GEOMETRICAL MOCKUP CONSISTS OF TWO ELLIPTICAL CYLINDERS REPRESENTING HEAD AND TRUNK.

(3) HISTOGRAMS HAVE 100 BINS, LOGARITHMICALLY SPACED.

(4) NUMBERS IN PARENTHESIS ARE STANDARD DEVIATIONS.

(5) THESE CALCULATIONS INVOLVED 5000 SAMPLES; OTHERS INVOLVED 500 SAMPLES.

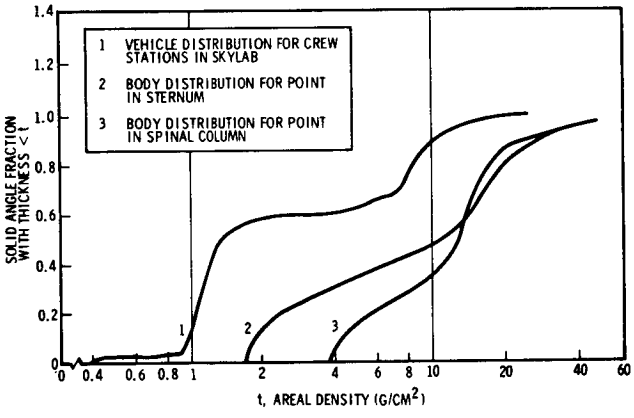

Figure 1. Typical Mass Distributions for Vehicle and Organ Segments

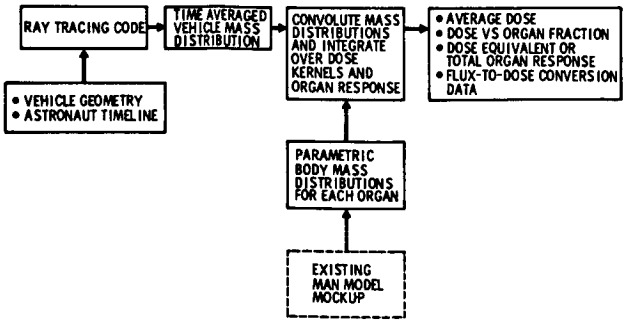

Figure 2. Technique for Dose Evaluation

16. Yucker, W. R.: Solar Cosmic Ray Hazard to Interplanetary and Earth-Orbital Space Travel. Proceedings of this symposium.

17. Holly, F. E.; and Janni, J. F.: Space Radiation Dosimetry. Aerospace Medicine, Vol. 40, No. 12, December 1969, pp. 1462-1475.

18. Sondhaus, C. A.; and Evans, R. D.: Dosimetry of Radiation in Space Flight. Radiation Dosimetry, Vol. III, Academic Press, Inc. (New York), 1969, pp. 453-521.

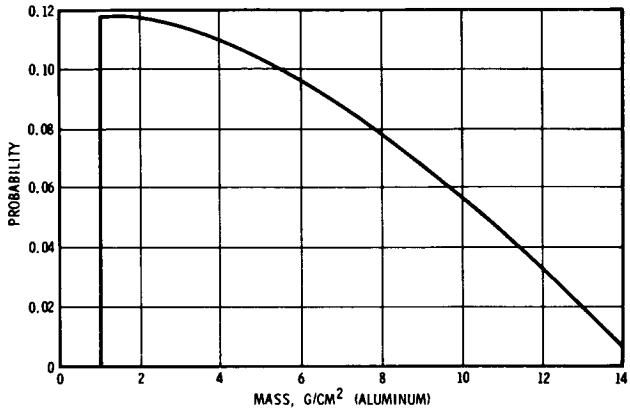

Figure 3. Mass Probability Density Function used in Statistical Analysis

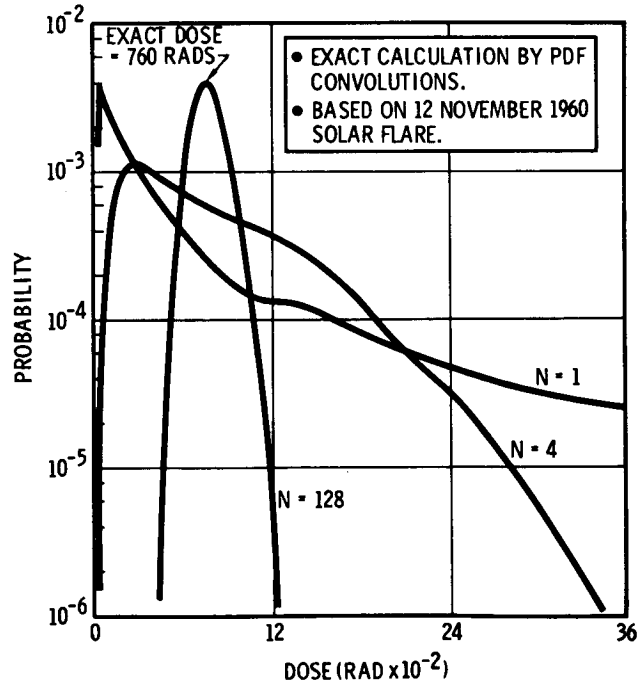

Figure 4. Dose Probability Distribution for N Random Rays

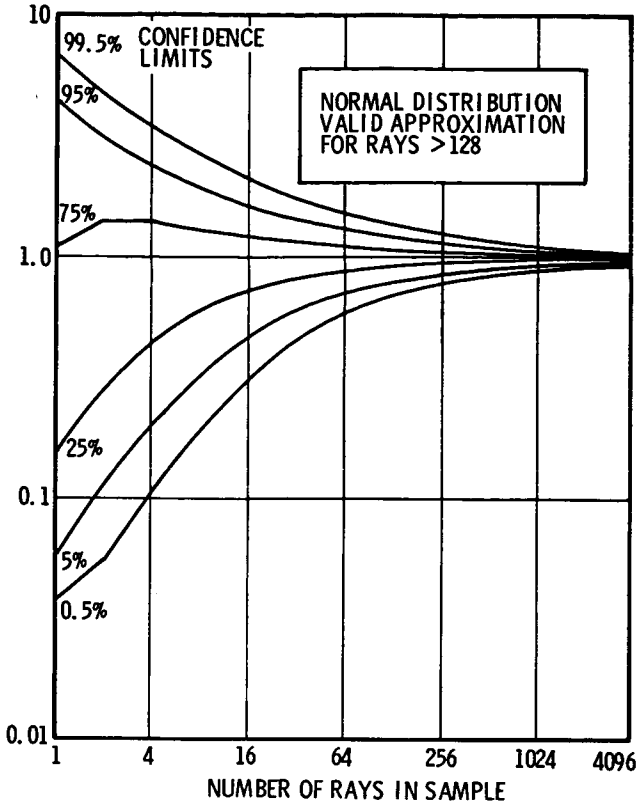

Figure 5. Confidence Intervals as a Function of Number of Random Rays

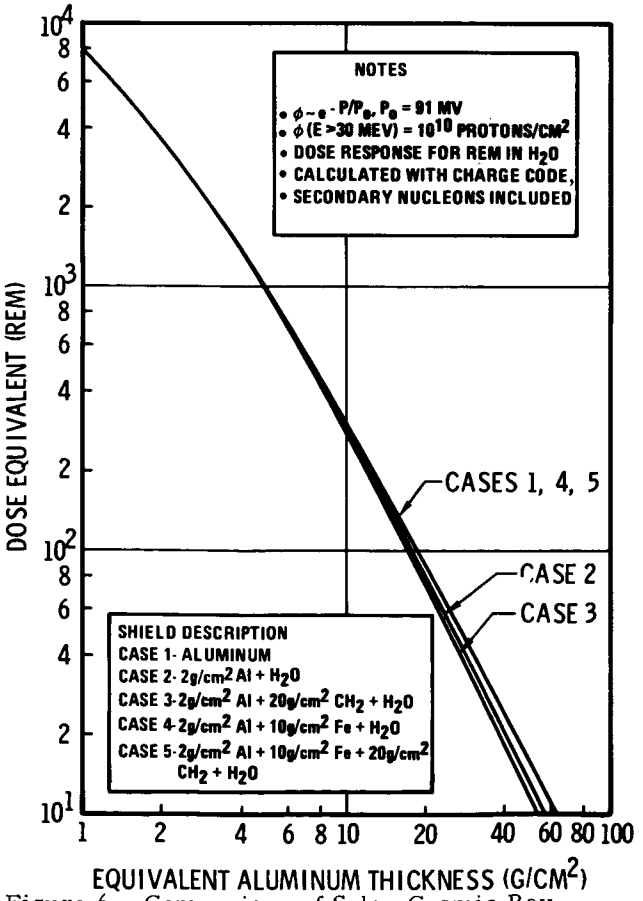

Figure 6. Comparison of Solar Cosmic Ray Dose Attenuation Kernels using Equivalent Aluminum Thickness

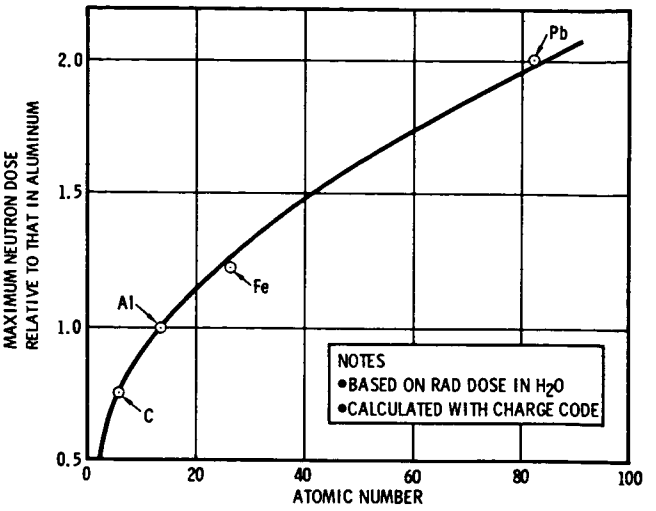

Figure 7. Relative Proton Shielding Effectiveness

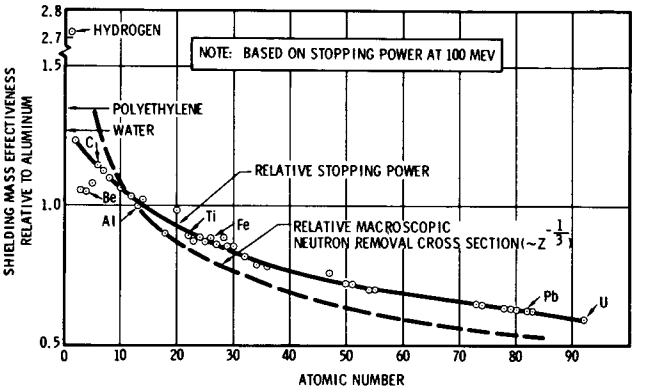

Figure 8. Secondary Neutron Dose Production as a Function of Atomic Number

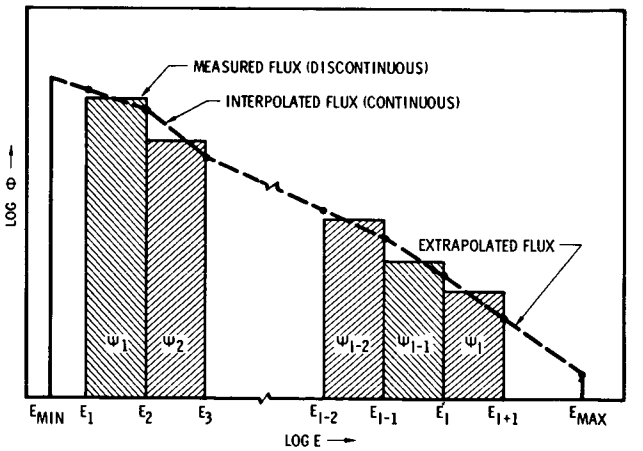

Figure 9. Flux Spectrum Representation

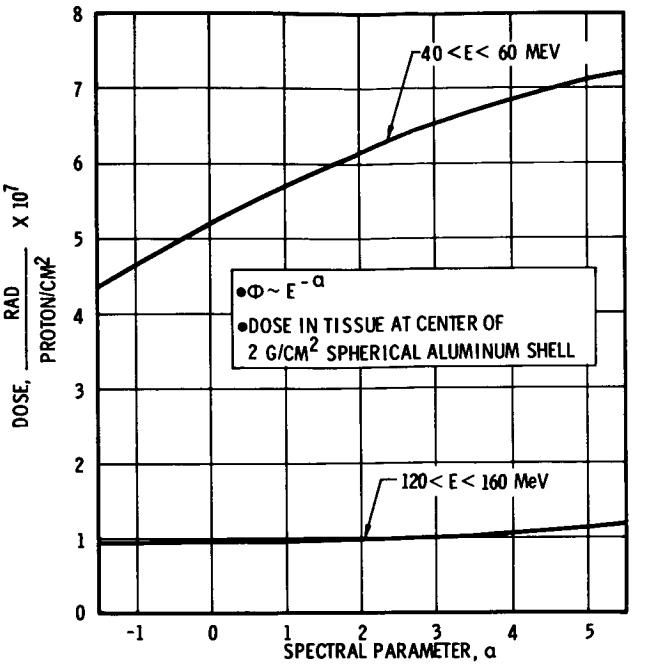

Figure 10. Example of Dose Conversion Versus Spectral Parameter